Reduction of Wave Propagation Loss by Mesh in Rectangular Tunnels

Yoshio Yamaguchi, *Member, IEEE*, Takemitsu Honda, and Masakazu Sengoku, *Member, IEEE*

Abstract— **The reduction of radio wave attenuation in rectangular tunnels is discussed. The attenuation of the dominant mode due to its field penetration into a lossy dielectric wall is reduced by means of the attachment of wire netting (mesh). First, a reflection coefficient from a mesh screen over a lossy surface is analytically evaluated. Then, based on a geometrical optical approach to the propagation model in tunnels, the attenuation of the dominant mode in a rectangular tunnel is derived using the reflection coefficient. The calculated attenuation constants are in good agreement with experimental ones obtained in a laboratory. Finally, the efficiency of attenuation reduction rate by the mesh shielding method is summarized as a function of spatial ratio of the mesh wire interval divided by the wavelength. It is shown that the efficiency of reduction rate by mesh is significant.**

Index Terms— **Tunnel, waveguide, attenuation constant, propagation loss, mesh.**

I. Introduction

The reduction of electromagnetic wave attenuation along a tunnel-like structure is important because it serves an expansion of radio communications capability in mobile, personal, and message communications, in addition to local security communications in closed spaces [1]–[20]. The structure includes not only road and railway tunnels, but also underground streets, corridors in buildings, coal mines, etc. However, only a few studies [19], [20] on the reduction of attenuation have been carried out. This paper extends the earlier work [19] and investigates the efficiency of wire netting on wall to reduce the attenuation characteristics in hollow tunnels. From the outset, we know that a straight tunnel can be regarded as a hollow waveguide surrounded by a lossy medium, and that for the propagation characteristics, the following is true.

1) The attenuation constant is due to refraction loss and ohmic loss in the surrounding walls whose dielectric properties vary with frequency [1].
2) The refraction loss plays a dominant role in the attenuation characteristics at higher frequencies where the wavelength is much smaller than the cross-sectional dimension, because the surrounding material acts as a pure dielectric at frequencies above the UHF band. There exist a high number of modes in tunnels in this higher frequency region, however, the lowest attenuated mode is the dominant mode whose attenuation constant is inversely proportional to the frequency squared and to the cubic size of the cross-sectional dimension [2], [3].
3) The ohmic loss plays a dominant role at lower frequencies when the wavelength is comparable to the tunnel dimension, because the surrounding material tends to act as a heavily lossy dielectric as the electromagnetic field penetrates into the surrounding medium resulting in the ohmic loss [4].

The reduction is less important in the higher frequency region where the wavelength is much smaller than the tunnel dimension because the attenuation constant itself is very small. On the other

Manuscript received April 1, 1993; revised March 1, 1994. This work was supported in part by the Telecommunications Advancement Foundation.

The authors are with the Department of Information Engineering, Faculty of Engineering, Niigata University, Ikarashi 2-8050, Niigata-shi 950-21, Japan.

IEEE Log Number 9407389.

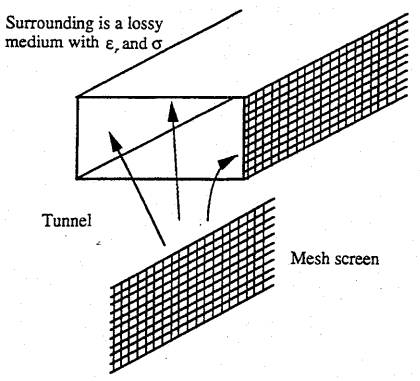

Fig. 1. Tunnel with mesh screen on inner surfaces.

hand, in the lower frequency region where the wavelength is close to the tunnel dimension, we encounter the propagation mode with large attenuation. It is our purpose to reduce the attenuation constant of the dominant mode in this frequency region where the ratio of cross-sectional tunnel dimension/wavelength ranges approximately from 0.6 to 5. The main factor that contributes to the attenuation in this frequency region is the penetration of the electromagnetic field into the surrounding material which finally results in the ohmic loss. Hence, the basic idea to reduce the attenuation is to limit the penetration of the field into the lossy walls, which leads to use of shielding techniques [20].

For the shielding purpose, [19] discusses the effect of periodical metallic strips placed on walls using boundary element method. It is shown that the reduction rate is determined mainly by the area percentage of strips. However, it is difficult to place strips on tunnel wall surfaces. The alternative (and most efficient) way seems to be to employ mesh for shielding. In this paper, we investigate the fundamental effect of a mesh screen placed on tunnel walls (Fig. 1) on the attenuation constant. The mesh screen consists of infinitely thin wires orthogonal to each other, i.e., rectangular mesh. Since a rigorous analysis considering all boundary conditions, including arbitrary cross-sectional tunnel shape, is extremely difficult, the propagation characteristics in a rectangular tunnel are analyzed based on a geometrical approach [1], [2] using reflection coefficient. In the following, the analytical reflection coefficient of a rectangular mesh screen placed on a lossy dielectric medium with planar surface is presented in Section II. Then the calculated reflection coefficient is applied to determine the attenuation constant in Section III. A laboratory experiment was carried out to compare the calculated results and to show the effectiveness of this wire-netting method in Section IV. Two cases are considered: one is such that all surfaces of a rectangular tunnel are covered with mesh; and the other is that the tunnel surfaces are partially covered (on both side walls and ceiling). Finally, the efficiency of reduction by the method is summarized in Section V as a function of the ratio of wire interval divided by the wavelength.

II. Reflection From Mesh

In this section, the reflection coefficient from a mesh screen placed above a lossy dielectric medium is presented. Since the formulations are presented in [22] in detail, only a brief explanation is given here. The geometry of the problem is shown in Fig. 2. The wire is assumed to be infinite both in the x- and y-directions. Each wire is connected to another at the intersection. The wire interval in the x-direction is a, and is b in the y-direction. Also, the spacing between the mesh screen and the lossy medium is h. Assuming a plane wave is incident from the -z direction onto the mesh plane at an incidence angle θ

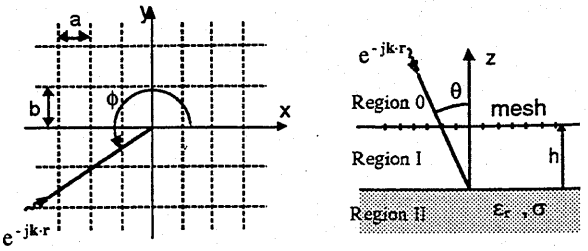

Fig. 2. Rectangular mesh on a lossy medium.

from the z-axis and at an angle ϕ with respect to the x-axis, the wave can be written as

$$\boldsymbol{E}_0 e^{j(\omega t - \boldsymbol{k}\cdot\boldsymbol{r})} \tag{1}$$

where

$$\boldsymbol{E}_0 = E_x\boldsymbol{x} + E_y\boldsymbol{y} + E_z z$$

$$\boldsymbol{k} = k_x\boldsymbol{x} + k_y\boldsymbol{y} - k_z z$$

$$k_x = -k\sin\theta\cos\phi, \qquad k_y = -k\sin\theta\sin\phi, \qquad k_z = k\cos\theta$$

$$k = \omega\sqrt{\epsilon_0\mu_0} = \frac{2\pi}{\lambda}$$

where ω is angular frequency, λ is wavelength in the free space, ϵ_0 is permittivity of the free space, μ_0 is permeability of the free space, and $\boldsymbol{x}$, $\boldsymbol{y}$, z are three orthogonal unit vectors.

The electric and magnetic Hertz vectors which determine the scattered field from the mesh screen are

$$\boldsymbol{\Pi}_e = \sum_{n=-\infty}^{\infty}\sum_{m=-\infty}^{\infty} \psi_{enm}(x, y)e^{\pm\Gamma_{nm}z}z \tag{2a}$$

$$\boldsymbol{\Pi}_h = \sum_{n=-\infty}^{\infty}\sum_{m=-\infty}^{\infty} \psi_{hnm}(x, y)e^{\pm\Gamma_{nm}z}z. \tag{2b}$$

Using Floquet's theorem, the Hertz potential function ψ in (2) can be expanded using the space harmonics as

$$\psi_{nm} = C_{nm}e^{-j\boldsymbol{k}_{\perp nm}\cdot\boldsymbol{\rho}} \tag{3}$$

where

$$\boldsymbol{\rho} = x\boldsymbol{x} + y\boldsymbol{y}$$

$$\boldsymbol{k}_{\perp nm} = k_{\perp xn}\boldsymbol{x} + k_{\perp ym}\boldsymbol{y}$$

$$k_{\perp xn} = k_x + \frac{2n\pi}{a}, \qquad k_{\perp ym} = k_y + \frac{2m\pi}{b}$$

$$\Gamma_{nm}^2 = \boldsymbol{k}_{\perp nm}\cdot\boldsymbol{k}_{\perp nm} - k^2 = k_{\perp nm}^2 - k^2. \tag{4}$$

In the following, the subscripts n and m, which are associated with modal quantities, will be omitted to simplify the notation. We divide the whole region into three subregions: 0 ($z > h$), I ($h > z > 0$), and II ($0 > z$). The field can be expanded in region 0 ($z > h$) as

$$H_z^0 = k_\perp^2\psi_h[e^{-\Gamma(z-h)} + R_h e^{-\Gamma(z+h)}] \tag{5a}$$

$$E_z^0 = -k_\perp^2\psi_e[e^{-\Gamma(z-h)} - R_e e^{-\Gamma(z+h)}] \tag{5b}$$

$$\boldsymbol{H}_\perp^0 = j\frac{\boldsymbol{k}_\perp\Gamma}{k_\perp^2}H_z^0 + j\frac{Y_e\Gamma}{k_\perp^2}(z\times\boldsymbol{k}_\perp)E_z^0 \tag{5c}$$

$$\boldsymbol{E}_\perp^0 = j\frac{\boldsymbol{k}_\perp\Gamma}{k_\perp^2}E_z^0 - j\frac{Z_h\Gamma}{k_\perp^2}(z\times\boldsymbol{k}_\perp)H_z^0 \tag{5d}$$

region I ($k > z > 0$) as

$$H_z^I = k_\perp^2 \psi_h [e^{\Gamma(z-h)} + R_h e^{-\Gamma(z+h)}] \tag{6a}$$

$$E_z^I = k_\perp^2 \psi_e [e^{\Gamma(z-h)} + R_h e^{-\Gamma(z+h)}] \tag{6b}$$

$$\boldsymbol{H}_\perp^I = -j\boldsymbol{k}_\perp \Gamma \psi_h [e^{\Gamma(z-h)} - R_h e^{-\Gamma(z+h)}] + jY_e \Gamma (z \times \boldsymbol{k}_\perp)\psi_e [e^{\Gamma(z-h)} + R_e e^{-\Gamma(z+h)}] \tag{6c}$$

$$\boldsymbol{E}_\perp^I = -j\boldsymbol{k}_\perp \Gamma \psi_e [e^{\Gamma(z-h)} - R_e e^{-\Gamma(z+h)}] - jZ_h \Gamma (z \times \boldsymbol{k}_\perp)\psi_h [e^{\Gamma(z-h)} + R_h e^{-\Gamma(z+h)}] \tag{6d}$$

region II ($0 > z$) as

$$H_z^{II} = T_h k_\perp'^2 \psi_h e^{(\Gamma' z - \Gamma h)} \tag{7a}$$

$$E_z^{II} = T_e k_\perp'^2 \psi_e e^{(\Gamma' z - \Gamma h)} \tag{7b}$$

$$\boldsymbol{H}_\perp^{II} = -j\frac{\boldsymbol{k}_\perp' \Gamma'}{k_\perp'^2} H_z^{II} + j\frac{Y_e' \Gamma'}{k_\perp'^2}(z \times k_\perp') E_z^{II} \tag{7c}$$

$$\boldsymbol{E}_\perp^{II} = -j\frac{\boldsymbol{k}_\perp' \Gamma'}{k_\perp'^2} E_z^{II} - j\frac{Z_h' \Gamma'}{k_\perp'^2}(z \times \boldsymbol{k}_\perp') H_z^{II} \tag{7d}$$

where prime $'$ indicates the quantity in the region II. The coefficients Y_e and Z_h in (5)–(7) are defined as follows:

$$Y_e = j\frac{\omega\epsilon}{\Gamma}, \qquad Z_h = j\frac{\omega\mu}{\Gamma}. \tag{8}$$

The boundary condition at $z = 0$, i.e., the continuity of tangential electric and magnetic field, imposes the following relation:

$$\boldsymbol{k}_\perp = \boldsymbol{k}_\perp' \tag{9a}$$

$$R_h = \frac{Z_h' - Z_h}{Z_h' + Z_h}, \qquad R_e = \frac{Y_e' - Y_e}{Y_e' + Y_e} \tag{9b}$$

$$T_h = \frac{\Gamma(1 - R_h)}{\Gamma'}, \qquad T_e = \frac{\Gamma(1 - R_e)}{\Gamma'}. \tag{9c}$$

Also, the boundary condition at $z = h$ is the discontinuity in the magnetic field, which is equal to the current flowing on the wire. If we expand the current using Fourier series in the x- and y-direction as

$$\boldsymbol{J}_s = \sum_{n=-\infty}^{\infty}\sum_{m=-\infty}^{\infty}\left[\left(\frac{I_{xn}}{b}\right)\boldsymbol{x} + \left(\frac{I_{ym}}{a}\right)\boldsymbol{y}\right]\exp(-j\boldsymbol{k}_{\perp nm}\cdot\boldsymbol{\rho}) \tag{10}$$

the boundary condition becomes

$$[z \times (\boldsymbol{H}_\perp^0 - \boldsymbol{H}_\perp^I)]_{nm} = \left[\left(\frac{I_{xn}}{b}\boldsymbol{x} + \frac{I_{ym}}{a}\boldsymbol{y}\right)\right]e^{-j\boldsymbol{k}_{\perp nm}\cdot\boldsymbol{\rho}}. \tag{11}$$

Therefore, Hertzian potentials for each mode can be obtained as below

$$\psi_e = \frac{1}{2j\Gamma k_\perp^2 Y_e}\left[\frac{k_{\perp xn} I_{xn}}{b} + \frac{k_{\perp ym} I_{ym}}{a}\right]e^{-j\boldsymbol{k}_\perp\cdot\boldsymbol{\rho}} \tag{12}$$

$$\psi_h = \frac{1}{2j\Gamma k_\perp^2}\left[-\frac{k_{\perp ym} I_{xn}}{b} + \frac{k_{\perp xn} I_{ym}}{a}\right]e^{-j\boldsymbol{k}_\perp\cdot\boldsymbol{\rho}}. \tag{13}$$

If the surface impedance boundary condition is applied to the current on a thin circular wire of radius r,

$$E = Z_i I \tag{14}$$

$$Z_i = \sqrt{\frac{\omega\mu_1}{2\sigma_1}}\left(\frac{1+j}{2\pi r}\right), \qquad \text{for } \sigma_1 \gg \omega\mu_1 \tag{15}$$

where μ_1 is permeability of wire, σ_1 is conductivity of wire, and r is radius of wire, it is possible to obtain the current both in the x- and y-direction. The reflection coefficient for the total structure is therefore given by

$$R_V = R_e + \left[\frac{k_x I_x}{2\omega\epsilon b} + \frac{k_y I_y}{2\omega\epsilon a}\right][e^{jk_z h} - R_e e^{-jk_z h}]/E_z^0(incident) \tag{16}$$

$$R_H = R_h + \left[\frac{k_y I_x}{2k_z b} - \frac{k_x I_y}{2k_z a}\right][e^{jk_z h} + R_h e^{-jk_z h}]/H_z^0(incident) \tag{17}$$

where

$$R_e = \frac{\epsilon_r^* \sin\varphi - \sqrt{\sin^2\varphi + \epsilon_r^* - 1}}{\epsilon_r^* \sin\varphi + \sqrt{\sin^2\varphi + \epsilon_r^* - 1}},$$

$$R_h = \frac{\sin\varphi - \sqrt{\sin^2\varphi + \epsilon_r^* - 1}}{\sin\varphi + \sqrt{\sin^2\varphi + \epsilon_r^* - 1}}$$

$$\epsilon_r^* = \frac{\epsilon}{\epsilon_0} - j\frac{\sigma}{\omega\epsilon_0} = \epsilon_r - j\epsilon_i, \qquad \varphi = \frac{\pi}{2} - \theta\text{: grazing angle}$$

where ϵ_r is the relative permittivity, σ is the conductivity of the dielectric medium, and $E_z^0(incident)$ and $H_z^0(incident)$ are the electric and magnetic fields incident in the region 0, respectively.

It should be noted that the first term is corresponding to Fresnel reflection coefficient due to the dielectric surface, and the second one is by the mesh structure. Higher order terms due to multiple reflections between the mesh and dielectric surface are neglected in (16) and (17) because the reflection coefficient from the mesh surface is large enough compared to that from dielectric surface, and the spacing between them is very small with respect to wavelength (the spacing is zero in the calculation). It is anticipated that the effect of multiple reflections is negligibly small.

Based on the above method, the reflection coefficients are calculated for the experimental condition:

frequency = 6 and 12 GHz
medium II: permittivity $\epsilon_r = 1.3$, conductivity $\sigma = 0.17$ S/m,
mesh screen: $a = b = d = 4$ mm, radius of wire $r = 0.35$ mm,
conductivity of wire (copper) $\sigma_1 = 5.81 \times 10^7$ S/m,
spacing between the mesh and the surface $h = 0.35$ mm.

The calculated result is shown in Figs. 3 and 4 with typical angle ϕ. The TE wave has the electric field perpendicular to the plane of incidence, and the TM wave has its electric field parallel to the plane of incidence. The following is observed in Figs. 3 and 4.

1) The magnitude of both reflection coefficients becomes large, and the Brewster angle for the TM wave approaches 90° by the attachment of mesh screen.
2) The reflection amplitude from mesh decreases as frequency increases. This is due to the change of a spatial ratio a/λ. If the ratio a/λ is small, the mesh surface behaves like a metal plate, which is one of the main topics in this work.
3) The reflection magnitude decreases as the angle ϕ increases. This is caused by the generation of cross-polarized component. However, the angle ϕ far from 0° does not contribute to propagation analysis in the tunnel which follows.

III. Attenuation Analysis by the Ray Approach

The attenuation constant of the dominant mode may be calculated by the ray method using reflection coefficient as shown in Fig. 5. The rectangular tunnel has a width d_1, and height d_2. A wave propagating in tunnels can be regarded as a ray which bounces from wall to wall making grazing angle φ_1 with the side walls, and φ_2 with the floor and the ceiling as seen in Fig. 5. This modeling is valid for a tunnel

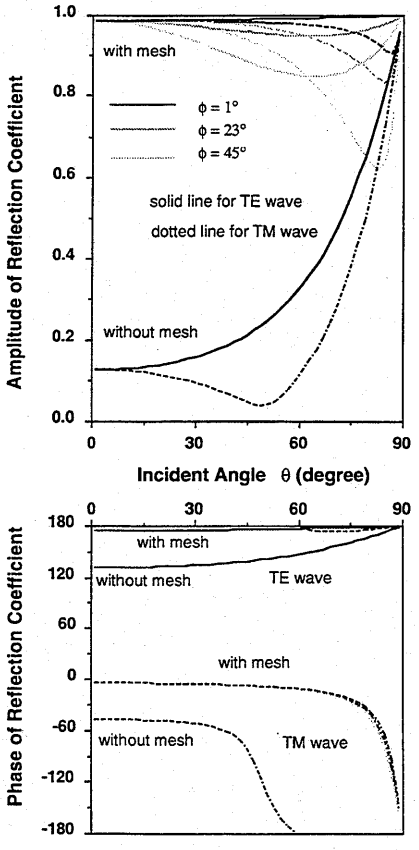

Fig. 3. TE and TM reflection coefficients for $4\times4-$mm-square mesh screen 0.35 mm above a lossy surface evaluated at 6 GHz.

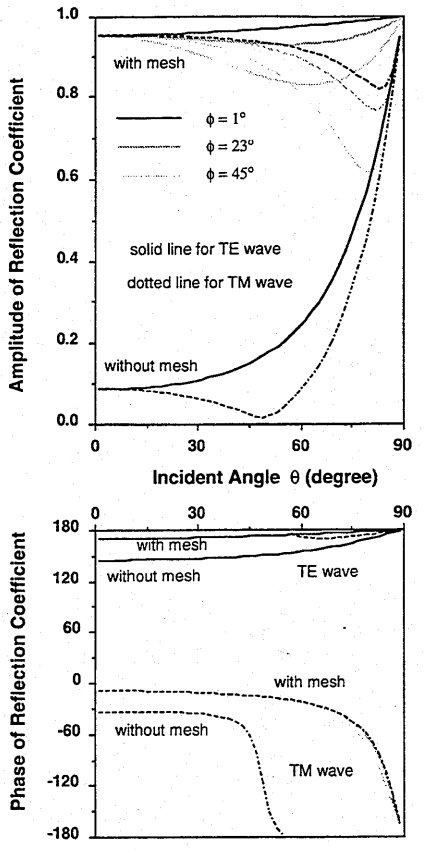

Fig. 4. TE and TM reflection coefficients for $4\times4-$mm-square mesh screen 0.35 mm above a lossy surface evaluated at 12 GHz.

whose cross section is more than two wavelengths. Assuming that the phase shift of wave is 2π after successive reflections on two walls, it can be derived that the incident angle θ and grazing angle φ satisfy the following equation:

$$\cos\theta_i = \sin\varphi_i = \frac{\lambda}{2d_i}. \qquad \varphi_i = \sin^{-1}\frac{\lambda}{2d_i} \qquad (i = 1.\ 2). \quad (18)$$

Since the numbers of reflections at a interval of z is given by

$$N_i = \frac{z\tan\varphi_i}{d_i} \quad (19)$$

the attenuation factor for the ray intensity for this distance is

$$\frac{I}{I_0} = (R_1^{N_1}R_2^{N_2})^2$$

where R_1 and R_2 are the reflection coefficients of the vertical and horizontal surfaces at the grazing angle φ_1 and φ_2, respectively. The propagation loss per unit length (attenuation constant) in the z-direction is therefore given by

$$\alpha = -10\log(|R_1|^{2N_1}|R_2|^{2N_2})/z$$
$$= -20\left(\frac{\tan\varphi_1}{d_1}\log|R_1| + \frac{\tan\varphi_2}{d_2}\log|R_2|\right). \quad (20)$$

It should be noted in (20) that the main factor contributing to the attenuation is the reflection coefficient if an operating frequency is given. The attenuation constant decreases as the reflection coefficient increases. Hence, it is possible to reduce attenuation by a mesh screen because of its high reflectivity.

There are two dominant modes for a rectangular tunnel. One is the vertically polarized mode with its principal electric field in the vertical direction d_2, which we refer to as the E_v mode. Another is the E_h mode with the electric field in the horizontal direction d_1.

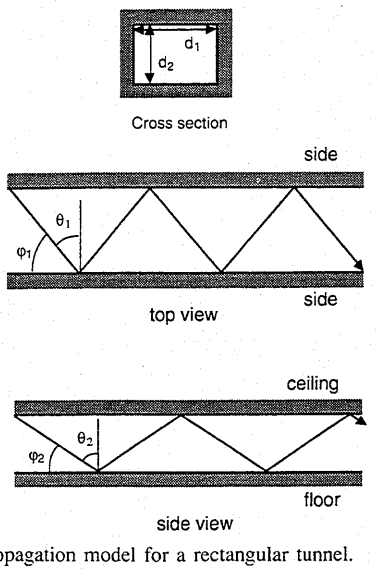

Fig. 5. Ray propagation model for a rectangular tunnel.

For the vertically polarized E_v mode, the reflection coefficient R_1 on side walls is given by (17), and the reflection coefficient R_2 on the ceiling and the floor by (16). And for the horizontally polarized E_h mode, R_1 is given by (16) and R_2 by (17), respectively.

IV. Laboratory Experiment

In order to confirm these theoretical results, we carried out a laboratory measurement on the attenuation constant. Fig. 6 shows the block diagram of the measurement scheme. A rectangular tunnel was employed which consisted of polystyrene foam combined with carbon

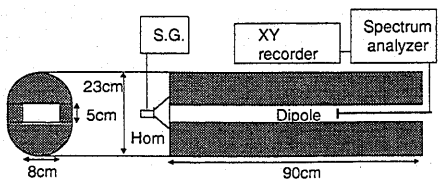

Fig. 6. Measurement setup.

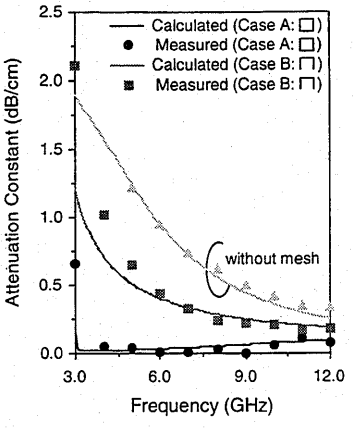

(a)

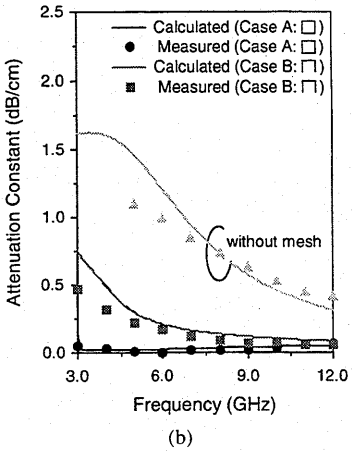

(b)

Fig. 7. Frequency characteristics of the attenuation constant: (a) horizontally polarized E_h mode, (b) vertically polarized E_v mode.

(10 g/L). The permittivity is 1.3, and the conductivity is 0.17 S/m. The tunnel size is 8 cm in width, 5 cm in height, and 90 cm in length. Two cases are considered. Case A is such that all surfaces of a rectangular tunnel are covered with mesh screen, which is denoted as a symbol "□." Case B is the partially covered (mesh on both side walls and on ceiling), denoted as "⊓." The field strength along the center (i.e., center point of rectangular cross section) line of the tunnel was picked up by a small dipole antenna 12 mm long, connected to a spectrum analyzer. This receiving antenna was moved continuously by hand with a precise position sensor. The field strength variation along the tunnel is thus recorded in an X-Y recorder. The attenuation constant is determined from the slope of field strength versus distance. Care was taken in the determination of the attenuation constant because the field strength distribution near the transmitting antenna and the tunnel exit does not show a regular pattern due to interference of higher mode excitation and reflection from the exit, respectively. Therefore, the section with regular pattern, where the field strength in dB is proportional to distance, was chosen for the determination of the attenuation constant. The section length is dependent on frequency, and was approximately 70 cm for 6 GHz.

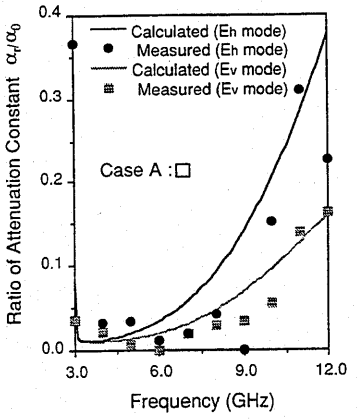

Fig. 8. Ratio of attenuation constant α_r/α_0, where α_r is the attenuation constant with mesh and α_0 is without mesh. All tunnel surfaces are covered with mesh screen in case A.

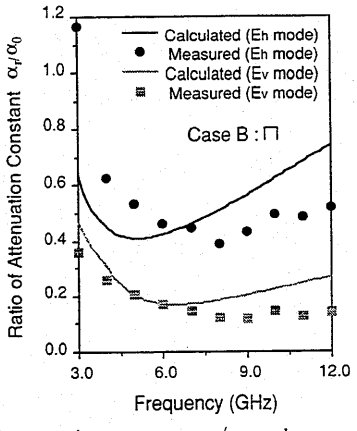

Fig. 9. Ratio of attenuation constant α_r/α_0, where α_r is the attenuation constant with mesh screen and α_0 is without mesh. Side walls and ceiling are covered with mesh screen in case B. The difference between case A is the absence of floor mesh.

Both theoretical and measured attenuation constants are shown in Fig. 7, where the attenuation constant without mesh is also illustrated. The theoretical attenuation constant without mesh is obtained by solving the characteristic equation [14] in the lower frequency region where a ray theory is not applicable. And the attenuation with mesh screen is derived from (20) which seems valid for frequencies higher than 6 GHz (i.e., in the frequency region where ray theory holds). It is seen that the theoretical attenuation constants are in good agreement with the experimental ones, even in the frequencies lower than 6 GHz. A significant reduction of attenuation constant by the mesh can be seen in this figure. The reduction rates obtained in this measurement are depicted in Fig. 8 for case A and in Fig. 9 for case B. The reduction ratio here is defined as α_r/α_0, where α_r is the attenuation constant with mesh, and α_0 is the attenuation constant without mesh in the hollow tunnel. The reduction efficiency is much higher than that obtained by strip attachment (see [19], for which the reduction rate is determined mainly by the area percentage of strips).

V. Reduction Efficiency by Mesh

The efficiency of attenuation reduction by mesh is calculated as a function of the spatial ratio of the wire interval divided by the wavelength. Since the attenuation constant in a tunnel is dependent on many parameters, it is difficult to define a unified efficiency taking

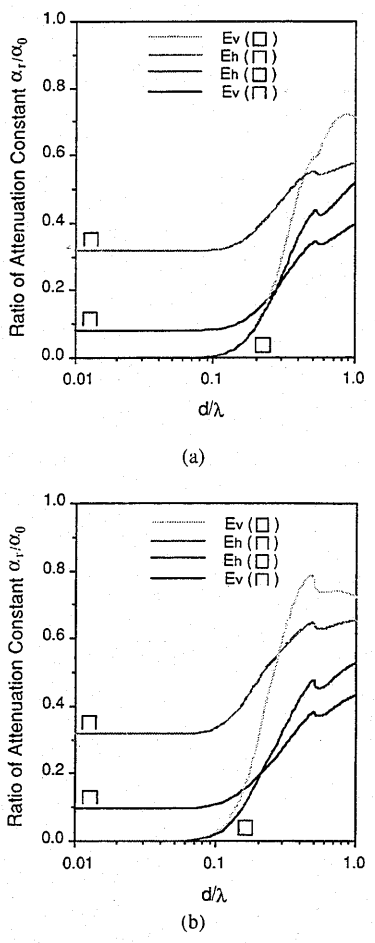

Fig. 10. Ratio of attenuation constant as a function of mesh interval/wavelength (d/λ): (a) tunnel size = 1λ(height) × 2λ(width), (b) tunnel size = 3λ(height) × 6λ(width).

account of all parameters. So, we took a parameter of spatial ratio, d/λ, for the efficiency calculation, assuming the mesh interval is the same ($a = b = d$). Fig. 10 shows the ratio of attenuation constant α_r/α_0 for two tunnel cross sections as a function of d/λ. Fig. 10(a) corresponds to the lower limiting case where the ray theory may hold, and Fig. 10(b) corresponds to the case for a large tunnel. Also, the attenuation ratio for fully covered (case A) and partially covered (case B) is depicted to show the difference. A significant reduction can be seen for $0.1 > d/\lambda$ regardless of tunnel size, for both cases A and B. For the case B "⊓," the remaining attenuation in the region $0.1 > d/\lambda$ is due to the loss on the tunnel floor. It is understood that the mesh screened wall behaves like a metallic plate for $0.1 > d/\lambda$. The condition $0.1 > d/\lambda$ is satisfied for ordinary mesh for the frequencies form VHF to microwave region.

These curves do not increase monotonically with d/λ. A sudden change around $d/\lambda = 0.5$ is caused by a resonant phenomenon in the tunnel.

VI. Conclusion

A mesh-netting technique for the reduction of the attenuation constant for the dominant mode in rectangular tunnels was presented. The electromagnetic field penetration into the surrounding wall is suppressed by mesh screen placed on the walls, which leads to a reduction of the propagation loss. The mesh netting is particularly effective when the wire interval is less than 0.1 wavelength in the lower frequency region where the wavelength and tunnel dimension are comparable, because a tunnel with mesh tends to act as a metallic waveguide.

Based on a geometrical optical approach to the propagation models, the attenuation constant in tunnels with the mesh-netting method was derived. The experimental results in a laboratory were in a good agreement with the calculated ones. However, a further study must be carried out to evaluate the attenuation characteristics in tunnels with bends and other cross sections, and will be treated in the future.

References

[1] S. F. Mahmoud and J. R. Wait, "Geometrical optical approach for electromagnetic propagation in rectangular mine tunnels," *Radio Sci.*, vol. 9, no. 12, pp. 1147–1158, 1974.

[2] A. G. Emslie, L. L. Robert, and P. F. Strong, "Theory of the propagation of UHF radio waves in coal mine tunnels," *IEEE Trans. Antennas Propagat.*, vol. AP-23, pp. 192–205, Mar. 1975.

[3] J. Chiba, T. Inaba, Y. Kuwamoto, O. Banno, and R. Sato, "Radio communication in tunnels," *IEEE Trans. Microwave Theory Tech.*, vol. MTT-26, pp. 439–443, June 1978.

[4] Y. Yamaguchi, T. Abe, and T. Sekiguchi, "Propagation characteristics of normal modes in hollow circular cylinder surrounded by dissipative medium," *Trans. IECE Japan*, vol. 62-B, no. 4, pp. 368–373, 1979.

[5] S. Kozono, T. Suzuki, and T. Hanazawa, "Experimental study of mobile radio propagation characteristics in rectangular tunnels," *Trans. IECE Japan*, vol. J62-B, no. 6, pp. 565–572, June 1979.

[6] Y. Yamaguchi, T. Abe, and T. Sekiguchi, "Propagation characteristics of the dominant mode in tunnels," *Trans. IECE Japan*, vol. J65-B, no. 4, pp. 471–476, Apr. 1982.

[7] K. Yasumoto and H. Shigematsu, "Analysis of propagation characteristics of radio waves in tunnels using surface impedance approximation," *Radio Sci.*, vol. 19, no. 2, pp. 597–602, 1984.

[8] B. Jacard and O. Maldonado, "Microwave modeling of rectangular tunnels," *IEEE Trans. Microwave Theory Tech.*, vol. MTT-32, pp. 576–581, 1984.

[9] Y. Yamaguchi, T. Abe, T. Sekiguchi, and J. Chiba, "Attenuation constants of UHF radio waves in arched tunnels," *IEEE Trans. Microwave Theory Tech.*, vol. MTT-33, pp. 714–718, Aug. 1985.

[10] K. Uchida, T. Matsunaga, K. Yoshidomi, and K. Aoki, "Electromagnetic wave excitation in a two-dimensional tunnel by waveguide modes," *Trans. IECE Japan*, E68, no. 3, pp. 159–165, Mar. 1985.

[11] K. Uchida, T. Matsunaga, and T. Noda, "Electromagnetic wave excitation in a two-dimensional impedance tunnel with a cross-junction," *Trans. IEICE Japan*, E70, no. 7, pp. 634–639, July 1987.

[12] T. Matsunaga, K. Uchida, and T. Noda, "Electromagnetic wave propagation in a two-dimensional tunnel," *Trans. IEICE Japan*, vol. J72-B-II, no. 1, pp. 26–33, Jan. 1989.

[13] ——, "Electromagnetic wave propagation in a two-dimensional tunnels with modified multi-cross-junctions," *Trans. IEICE Japan*, vol. J72-B-II, no. 8, pp. 390–395, Aug. 1989.

[14] Y. Yamaguchi, T. Abe, and T. Sekiguchi, "Experimental study of radio propagation characteristics in an underground street and corridors," *IEEE Trans. Electromagn. Compat.*, vol. EMC-28, pp. 148–155, Aug. 1986.

[15] ——, "Radio propagation characteristics in underground streets crowded with pedestrians," *IEEE Trans. Electromagn. Compat.*, vol. EMC-30, pp. 130–1136, May 1988.

[16] ——, "Radio propagation loss in the VHF to microwave region due to vehicles in tunnels," *IEEE Trans. Electromagn. Compat.*, vol. EMC-31, pp. 87–91, Feb. 1989.

[17] K. Sakai and M. Koshiba, "Application of the boundary-element method to an infinitely long tunnel," *Trans. IEICE Japan*, vol. J-71-B, no. 7, pp. 872–881, 1988.

[18] ——, "Analysis of electromagnetic field distribution in tunnels with partition walls," *Trans. IEICE Japan*, vol. J72-B-II, no. 11, pp. 595–602, 1989.

[19] Y. Yamaguchi, T. Honda, M. Sengoku, S. Motooka, and T. Abe, "On the reduction of wave propagation loss in tunnels," *IEEE Trans. Electromagn. Compat.*, vol. 34, pp. 78–85, May 1992.

[20] Y. Yamaguchi, T. Abe, and T. Sekiguchi, "Improvement of attenuation characteristics in tunnels (II)," *Tech. Rep. IECE*. EMCJ 83-48, Oct. 1983.

[21] J. R. Wait, "Theories of scattering from wire grid and mesh structures," in *Electromagnetic Scattering*, P. L. E. Uslenghi, Ed. New York: Academic, 1978, pp. 253–287.

[22] G. A. Otteni, "Plane wave reflection from a rectangular mesh ground screen," *IEEE Trans. Antennas Propagat.*, vol. AP-21, pp. 843–851, Nov. 1973.